Bulletin of the Institute of Mathematics
Academia Sinica (New Series)
Vol. **10** (2015), No. 3, pp. 423-448

SECOND-ORDER KNUDSEN-LAYER ANALYSIS FOR THE GENERALIZED SLIP-FLOW THEORY I

MASANARI HATTORI[1,a] AND SHIGERU TAKATA[2,b]

[1]Department of Mechanical Engineering and Science, Kyoto University, Kyoto 615-8540, Japan.
[a]E-mail: hattori.masanari.32s@st.kyoto-u.ac.jp
[2]Department of Aeronautics and Astronautics & Advanced Research Institute of Fluid Science and Engineering, Kyoto University, Kyoto 615-8540, Japan.
[b]E-mail: takata.shigeru.4a@kyoto-u.ac.jp

Abstract

Numerical analyses of the second-order Knudsen layer are conducted on the basis of the linearized Boltzmann equation for hard-sphere molecules under the diffuse reflection boundary condition. These aim at completing the data for the asymptotic theory of the Boltzmann equation (the generalized slip-flow theory) that have been lacking for nearly a half century except for the Bhatnagar–Gross–Krook (or Boltzmann–Krook–Welander) kinetic model equation. Numerical data, except for the curvature effects, are prepared up to the second order in the Knudsen number expansion.

1. Introduction

Study on the connection between the kinetic theory and the fluid-dynamics has a long history [3, 8, 7] and a number of important results have been obtained for a small or a vanishing limit of the Knudsen number, e.g., [5, 6, 17, 18, 19, 28]. Mathematical studies are developing to include the argument of boundary condition for the fluid-dynamical equation [4, 10, 12]. It seems, however, that they are mainly concerned with the vanishing limit of the Knudsen number and are not intended to describe the gas rarefaction effect itself. In the meantime, a systematic asymptotic theory established in the late 1960s and early 1970s [17, 18] and developed further since then [19]

Received January 21, 2015.
AMS Subject Classification: 35Q20, 76P05, 76M45, 82C40, 82D05.
Key words and phrases: Boltzmann equation, kinetic theory, slip flow, Knudsen number, rarefied gas.

provides not only the fluid-dynamic description in the bulk region but also the slip/jump boundary condition and the non-fluid-like correction in a thin layer adjacent to the boundary (the Knudsen layer) for small Knudsen numbers. We call the linear case of this theory the generalized slip-flow theory in the present paper. The generalized slip-flow theory contains rich information on the gas rarefaction effect, giving a fluid-dynamical interpretation to various phenomena occurring for small Knudsen numbers. It also motivates recent studies on time-dependent problems in the framework of the theory [9, 13, 25].

The theory has been applied to various fundamental problems and is revealed to be practical. However, such applications have been limited mostly to the studies based on the Bhatnagar–Gross–Krook (BGK) [or Boltzmann–Krook–Welander (BKW)] model equation [2, 26]. This is due to lack of numerical data at the second order of the Knudsen number for the original Boltzmann equation. Some difficulties in numerical analyses, which could be bypassed for the BGK model, have prevented the preparation of the desired data. Here, the difficulties do not mean a mere numerical cost but rather mean possible singularities inherent in the elemental (or component) half-space problems to be solved.

The present paper reports the first part of our recent attempts to prepare the missing data that are necessary in applying the theory to specific problems on the basis of the original Boltzmann equation. Assuming the hard-sphere molecules and the diffuse reflection boundary condition, we provide the data for the generalized slip-flow theory, up to the second order of the Knudsen number expansion, except for the curvature effects.

2. Generalized Slip-Flow Theory: An Outline

2.1. Physical setting

We consider a gas around smooth solid bodies which do not change in time their shape and position under the following assumptions: (i) There is no external force and the behavior of the gas is described by the Boltzmann equation for monatomic molecules; (ii) The gas molecules are reflected locally isotropically [19] on the surface of the solid bodies (no net flow across their surface); (iii) The deviation from the reference equilibrium state at rest with

density ρ_0 and temperature T_0 is so small that the equation and the initial and the boundary condition can be linearized around that equilibrium state; (iv) The mean free path ℓ_0 of a molecule at the reference equilibrium state is much smaller than the characteristic length L of the physical system (i.e., the Knudsen number $\mathrm{Kn} = \ell_0/L \ll 1$); (v) The time evolution is initiated by a slow change of the surroundings from the reference equilibrium state.

The time scale of the change t_0 in (v) is the same order as that of the viscous and the thermal diffusion, and we set it as $t_0 = (2/\sqrt{\pi})(L^2/\ell_0\sqrt{2RT_0})$, where R is the specific gas constant (the Boltzmann constant k divided by the mass of a molecule m). In the actual computations for the Knudsen-layer analysis, we assume the hard-sphere molecules in (i) and the diffuse reflection boundary condition in (ii). For hard-sphere molecules, $\ell_0 = [\sqrt{2}\pi d_m^2(\rho_0/m)]^{-1}$, where d_m is the diameter of a molecule.

2.2. Resulting framework

The generalized slip-flow theory consists of first considering the overall behavior of the gas that changes in the scale of the characteristic length (and time) of the system and then introducing the correction in the vicinity of the boundary. The first part is conducted by the Hilbert (or Grad–Hilbert) expansion to yield a set of fluid-dynamic equations. The solution of this set is called the Hilbert part (or solution). The second part is conducted by the expansion after rescaling (actually stretching) the spatial coordinate in the direction normal to the boundary. This yields a set of slip/jump boundary condition and the associated correction to the fluid-dynamic solution near the boundary. The correction is called the Knudsen-layer correction, which is the primary concern in the present paper.

Let us denote by Lx_i the space coordinates, by $t_0 t$ the time, by $\rho_0(1+\omega)$ the density of the gas, by $(2RT_0)^{1/2}u_i$ the flow velocity, by $T_0(1+\tau)$ the temperature, by $p_0(1+P)$ the pressure with $p_0 = \rho_0 RT_0$, and by $(2RT_0)^{1/2}u_{i\mathrm{w}}$ and $T_0(1+\tau_{\mathrm{w}})$ the velocity and the temperature of the body surface. Since solid bodies change neither the shape nor the position, $u_{i\mathrm{w}}n_i = 0$, where n_i is the unit vector normal to the surface, pointed to the gas. We denote the Hilbert part and the Knudsen-layer correction of the macroscopic quantity h ($h = \omega,\ u_i,\ \tau,\ P$) by h_{H} and h_{K}, respectively: $h = h_{\mathrm{H}} + h_{\mathrm{K}}$. Since the Knudsen number is small, we use $\varepsilon = (\sqrt{\pi}/2)\mathrm{Kn}$ as a small parameter. The

Hilbert part and the Knudsen-layer correction are obtained by a power series expansion in ε, which will be denoted as $h_{\rm H} = h_{\rm H0} + h_{\rm H1}\varepsilon + h_{\rm H2}\varepsilon^2 + \cdots$ and $h_{\rm K} = h_{\rm K0} + h_{\rm K1}\varepsilon + h_{\rm K2}\varepsilon^2 + \cdots$. Actually, the expansion of $h_{\rm K}$ starts from $O(\varepsilon)$, because no correction to the Hilbert solution is required at $O(1)$.

The resulting set of fluid-dynamic equations, their slip/jump boundary conditions, and the Knudsen-layer corrections up to the second order of the expansion in ε are summarized as follows: [25]

Fluid-dynamic equations

$$\frac{\partial P_{\rm H0}}{\partial x_i} = 0, \tag{2.1a}$$

$$\frac{\partial u_{i{\rm H}m}}{\partial x_i} + \frac{\partial \omega_{{\rm H}m-1}}{\partial t} = 0, \tag{2.1b}$$

$$\frac{\partial u_{i{\rm H}m}}{\partial t} + \frac{1}{2}\frac{\partial P^*_{{\rm H}m+1}}{\partial x_i} - \frac{1}{2}\gamma_1\frac{\partial^2 u_{i{\rm H}m}}{\partial x_j^2} + \frac{1}{4}(\gamma_1\gamma_{10} - 2\gamma_6)\frac{\partial^4 u_{i{\rm H}m-2}}{\partial x_j^2 \partial x_k^2} = 0, \tag{2.1c}$$

$$\frac{\partial \tau_{{\rm H}m}}{\partial t} - \frac{2}{5}\frac{\partial P_{{\rm H}m}}{\partial t} - \frac{1}{2}\gamma_2\frac{\partial^2 \tau_{{\rm H}m}}{\partial x_j^2} + \frac{1}{10}\left(\gamma_2\gamma_3 - \frac{13}{2}\gamma_{11}\right)\frac{\partial^4 \tau_{{\rm H}m-2}}{\partial x_j^2 \partial x_k^2} = 0, \tag{2.1d}$$

$$P^*_{{\rm H}m+1} = P_{{\rm H}m+1} - \frac{1}{6}\left(\gamma_2\gamma_1 - 4\gamma_3\right)\frac{\partial^2 \tau_{{\rm H}m-1}}{\partial x_j^2} + \frac{1}{5}\gamma_1\frac{\partial P_{{\rm H}m-1}}{\partial t}, \tag{2.1e}$$

$$P_{{\rm H}m} = \omega_{{\rm H}m} + \tau_{{\rm H}m}, \tag{2.1f}$$

where $m = 0, 1, 2$ and the quantities $h_{\rm H-1}$ and $h_{\rm H-2}$ ($h = \omega, u_i, \tau, P$) should be read as zero. The γ's occurring in the equations are positive constants corresponding to the transport coefficients at the reference state; γ's are all unity for the BGK model, while they are respectively $\gamma_1 = 1.270042427$, $\gamma_2 = 1.922284066$, $\gamma_3 = 1.947906335$, $\gamma_6 = 1.419423836$, $\gamma_{10} = 1.63607346$, and $\gamma_{11} = 2.7931173$ for hard-sphere molecules.

Slip/jump boundary condition and the Knudsen-layer correction

$$\begin{aligned}
\begin{bmatrix} (u_{i{\rm H}m} - u_{i{\rm w}m})t_i \\ u_{i{\rm K}m}t_i \end{bmatrix} &= \overline{\frac{\partial u_{i{\rm H}m-1}}{\partial x_j}} n_i t_j \begin{bmatrix} b_1^{(1)} \\ Y_1^{(1)}(\eta) \end{bmatrix} + \frac{\partial \tau_{{\rm H}m-1}}{\partial x_i} t_i \begin{bmatrix} b_2^{(1)} \\ Y_2^{(1)}(\eta) \end{bmatrix} \\
&+ \frac{\partial^2 \tau_{{\rm H}m-2}}{\partial x_i \partial x_j} n_i t_j \begin{bmatrix} b_3^{(1)} \\ Y_3^{(1)}(\eta) \end{bmatrix} + \frac{\partial}{\partial x_i}\overline{\frac{\partial u_{j{\rm H}m-2}}{\partial x_k}} n_i n_j t_k \begin{bmatrix} b_4^{(1)} \\ Y_4^{(1)}(\eta) \end{bmatrix} \\
&+ \bar{\kappa}\overline{\frac{\partial u_{i{\rm H}m-2}}{\partial x_j}} n_i t_j \begin{bmatrix} b_5^{(1)} \\ Y_5^{(1)}(\eta) \end{bmatrix} + \kappa_{ij}\overline{\frac{\partial u_{j{\rm H}m-2}}{\partial x_k}} n_k t_i \begin{bmatrix} b_6^{(1)} \\ Y_6^{(1)}(\eta) \end{bmatrix}
\end{aligned}$$

$$+\kappa_{ij}\frac{\partial\tau_{\mathrm{H}m-2}}{\partial x_i}t_j\begin{bmatrix}b_7^{(1)}\\ Y_7^{(1)}(\eta)\end{bmatrix}+\bar\kappa\frac{\partial\tau_{\mathrm{H}m-2}}{\partial x_i}t_i\begin{bmatrix}b_8^{(1)}\\ Y_8^{(1)}(\eta)\end{bmatrix}, \tag{2.2a}$$

$$\begin{bmatrix}u_{i\mathrm{H}m}n_i\\ u_{i\mathrm{K}m}n_i\end{bmatrix}=\frac{1}{2}\frac{\partial}{\partial x_i}\overline{\frac{\partial u_{j\mathrm{H}m-2}}{\partial x_k}}n_in_jn_k\begin{bmatrix}\int_0^\infty Y_1^{(1)}(z)dz\\ -\int_\eta^\infty Y_1^{(1)}(z)dz\end{bmatrix}$$
$$+\left[2\bar\kappa\frac{\partial\tau_{\mathrm{H}m-2}}{\partial x_i}n_i-\frac{\partial^2\tau_{\mathrm{H}m-2}}{\partial x_i\partial x_j}(\delta_{ij}-n_in_j)\right]\begin{bmatrix}\int_0^\infty Y_2^{(1)}(z)dz\\ -\int_\eta^\infty Y_2^{(1)}(z)dz\end{bmatrix}, \tag{2.2b}$$

$$\begin{bmatrix}\tau_{\mathrm{H}m}-\tau_{\mathrm{w}m}\\ \omega_{\mathrm{K}m}\\ \tau_{\mathrm{K}m}\end{bmatrix}=\frac{\partial\tau_{\mathrm{H}m-1}}{\partial x_i}n_i\begin{bmatrix}c_1^{(0)}\\ \Omega_1^{(0)}(\eta)\\ \Theta_1^{(0)}(\eta)\end{bmatrix}+\frac{\partial u_{i\mathrm{H}m-1}}{\partial x_i}\begin{bmatrix}c_5^{(0)}\\ \Omega_5^{(0)}(\eta)\\ \Theta_5^{(0)}(\eta)\end{bmatrix}$$
$$+\frac{\partial^2\tau_{\mathrm{H}m-2}}{\partial x_i\partial x_j}(\delta_{ij}-n_in_j)\begin{bmatrix}c_2^{(0)}\\ \Omega_2^{(0)}(\eta)\\ \Theta_2^{(0)}(\eta)\end{bmatrix}+\frac{\partial^2\tau_{\mathrm{H}m-2}}{\partial x_j^2}\begin{bmatrix}c_6^{(0)}\\ \Omega_6^{(0)}(\eta)\\ \Theta_6^{(0)}(\eta)\end{bmatrix}$$
$$+\frac{\partial}{\partial x_i}\overline{\frac{\partial u_{j\mathrm{H}m-2}}{\partial x_k}}n_in_jn_k\begin{bmatrix}c_3^{(0)}\\ \Omega_3^{(0)}(\eta)\\ \Theta_3^{(0)}(\eta)\end{bmatrix}+\bar\kappa\frac{\partial\tau_{\mathrm{H}m-2}}{\partial x_i}n_i\begin{bmatrix}c_4^{(0)}\\ \Omega_4^{(0)}(\eta)\\ \Theta_4^{(0)}(\eta)\end{bmatrix}, \tag{2.2c}$$

$$P_{\mathrm{K}m}=\omega_{\mathrm{K}m}+\tau_{\mathrm{K}m}, \tag{2.2d}$$

where $m=0,1,2$ and $\overline{f_{ij}}=f_{ij}+f_{ji}-(2/3)f_{kk}\delta_{ij}$ (δ_{ij} is the Kronecker delta). In (2.2), the quantities with the subscript H or w denote their values at the (dimensionless) surface position $x_{i\mathrm{w}}$, and t_i (or n_i) is a unit vector tangential (or normal) to the surface at $x_{i\mathrm{w}}$. The quantities with the subscript K depend on η as well as $x_{i\mathrm{w}}$, where η is the stretched spatial coordinate normal to the surface at $x_{i\mathrm{w}}$ such that the position x_i in the Knudsen layer is expressed by $x_i=x_{i\mathrm{w}}+\varepsilon\eta n_i$. The surface velocity and temperature are also expanded in a power series of ε: $h_{\mathrm{w}}=h_{\mathrm{w}0}+h_{\mathrm{w}1}\varepsilon+h_{\mathrm{w}2}\varepsilon^2+\cdots$ ($h=u_i,\tau$). The effect of surface curvature occurs through the terms with κ's defined by

$$\bar\kappa=\frac{1}{2}(\kappa_1+\kappa_2),\quad \kappa_{ij}=\kappa_1\ell_i\ell_j+\kappa_2m_im_j. \tag{2.3}$$

Here κ_1/L and κ_2/L are the principal curvatures of the boundary, with κ_1 and κ_2 being taken negative when the corresponding center of curvature lies on the gas side; ℓ_i and m_i are the direction cosines of the principal directions corresponding to κ_1 and κ_2 respectively.

Many terms degenerate from (2.1) and (2.2) when $m = 0, 1$. For instance, the boundary condition at $O(1)$, namely for $m = 0$, is none other than the non-slip/non-jump condition; the slip/jump may occur at the first or higher order of ε. The reader is referred to [19, 25] for the discussions on the main features of the above system. The system can be solved from the lowest order to determine the time-dependent behavior of the gas under the considered situation, provided that the data of the slip/jump coefficients $c_1^{(0)} \sim c_6^{(0)}$, $b_1^{(1)} \sim b_8^{(1)}$, $\int_0^\infty Y_1^{(1)}(z)dz$, $\int_0^\infty Y_2^{(1)}(z)dz$ and the elemental (or component) Knudsen-layer functions $\Omega_1^{(0)}(\eta) \sim \Omega_6^{(0)}(\eta)$, $\Theta_1^{(0)}(\eta) \sim \Theta_6^{(0)}(\eta)$, $Y_1^{(1)}(\eta) \sim Y_8^{(1)}(\eta)$ are available. They are obtained by solving elemental (or component) half-space problems of the linearized Boltzmann equation, which may be homogeneous or inhomogeneous depending on that component.

2.3. Remaining issue

Since the first publication of the generalized slip-flow theory [17, 18], the complete set of the slip/jump coefficients and the associated Knudsen-layer corrections has been available only for the BGK model. For the original Boltzmann equation, difficulties in directly solving the component problems have prevented preparing the corresponding data. Even for hard-sphere molecules under the diffuse reflection condition, the component problems have been tackled only for the problems of temperature jump $(c_1^{(0)}, \Omega_1^{(0)}, \Theta_1^{(0)})$, shear slip $(b_1^{(1)}, Y_1^{(1)})$, thermal slip $(b_2^{(1)}, Y_2^{(1)})$, thermal-stress slip $(b_3^{(1)}, Y_3^{(1)})$, and thermal inertia due to time evolution $(c_6^{(0)}, \Omega_6^{(0)}, \Theta_6^{(0)})$ [14, 15, 20, 22].

Recently, we have succeeded in [25] to prepare the complete set of slip/jump coefficients up to the second order of ε by making use of the theory of symmetry relation [21]. This method is, however, indirect, and the information on the Knudsen-layer structure at the second order is still far from complete. In the present work, we numerically solve the component problems at the second order of ε. We shall focus on the component problems related to $(c_2^{(0)}, \Omega_2^{(0)}, \Theta_2^{(0)})$, $(c_3^{(0)}, \Omega_3^{(0)}, \Theta_3^{(0)})$, $(c_5^{(0)}, \Omega_5^{(0)}, \Theta_5^{(0)})$, and $(b_4^{(1)}, Y_4^{(1)})$ only. These problems might be handled by the finite-difference method as in [14]. Nevertheless, we take a new approach that makes use of the integral formulation of the Boltzmann equation, the formulation that has been effective in the study of singularities [23, 24]. The primary motivation of this approach is that the remaining component problems, which are

related to the curvature effect and left to a separate paper, contain a much delicate matter, requiring a new methodology for the numerical analysis.

3. Knudsen-Layer Problems

Let us denote by $(2RT_0)^{1/2}\boldsymbol{\zeta}$ the molecular velocity and introduce the notation $\zeta = |\boldsymbol{\zeta}|$ and $\mu = \zeta_i n_i/\zeta$, where $-1 \le \mu \le 1$ and $0 \le \zeta < \infty$. Then, the component problems for the Knudsen layer admit a similarity solution of three arguments (η, μ, ζ) and are reduced to the following two types of boundary-value problems by assuming the hard-sphere molecules and the diffuse reflection boundary condition:

$$\mu\zeta\frac{\partial\phi_\alpha}{\partial\eta} = -\nu(\zeta)\phi_\alpha + \mathcal{C}[\phi_\alpha] - \mathcal{I}_\alpha(\eta,\mu,\zeta), \tag{3.1a}$$

$$\phi_\alpha = -\sigma_\alpha^{(0)} - c_\alpha^{(0)}\zeta^2 + g_\alpha(\mu,\zeta), \quad (\mu\zeta > 0,\ \eta = 0), \tag{3.1b}$$

$$\phi_\alpha \to\ 0, \quad \text{as} \quad \eta \to \infty, \tag{3.1c}$$

and

$$\mu\zeta\frac{\partial\psi_\beta}{\partial\eta} = -\nu(\zeta)\psi_\beta + \mathcal{C}^S[\psi_\beta] - \mathcal{I}_\beta^S(\eta,\mu,\zeta), \tag{3.2a}$$

$$\psi_\beta = -2b_\beta^{(1)} + g_\beta^S(\mu,\zeta), \quad (\mu\zeta > 0,\ \eta = 0), \tag{3.2b}$$

$$\psi_\beta \to\ 0, \quad \text{as} \quad \eta \to \infty. \tag{3.2c}$$

Here

$$\nu(\zeta) = \frac{1}{2\sqrt{2}}\left[\exp(-\zeta^2) + \left(2\zeta + \frac{1}{\zeta}\right)\int_0^\zeta \exp(-\xi^2)d\xi\right];$$

$\mathcal{C}$ is an integral operator acting on a function of $\boldsymbol{\zeta}$ to be defined soon later; and g_α, $\mathcal{I}_\alpha$, g_β^S, and $\mathcal{I}_\beta^S$ are given functions. $\mathcal{I}_\alpha$ and $\mathcal{I}_\beta^S$ are supposed to decay fast in η. The solution ϕ_α (or ψ_β) ($\alpha = 1,\dots,6$; $\beta = 1,\dots,8$) is a function of η, μ, and ζ. It is determined together with the constants $\sigma_\alpha^{(0)}$ and $c_\alpha^{(0)}$ [or $b_\beta^{(1)}$] for every given $(\mathcal{I}_\alpha, g_\alpha)$ [or $(\mathcal{I}_\beta^S, g_\beta^S)$] [1]. The operator $\mathcal{C}$ is defined by

$$\mathcal{C}[\phi](\boldsymbol{\zeta}) = \int [k_1(\boldsymbol{\zeta},\boldsymbol{\xi}) - k_2(\boldsymbol{\zeta},\boldsymbol{\xi})]\phi(\boldsymbol{\xi})d\boldsymbol{\xi},$$

$$k_1(\boldsymbol{\zeta},\boldsymbol{\xi}) = \frac{1}{\sqrt{2}\pi|\boldsymbol{\zeta}-\boldsymbol{\xi}|}\exp\left(-|\boldsymbol{\xi}|^2 + \frac{|\boldsymbol{\xi}\times\boldsymbol{\zeta}|^2}{|\boldsymbol{\xi}-\boldsymbol{\zeta}|^2}\right),$$

$$k_2(\boldsymbol{\zeta}, \boldsymbol{\xi}) = \frac{|\boldsymbol{\zeta} - \boldsymbol{\xi}|}{2\sqrt{2}\pi} \exp\left(-|\boldsymbol{\xi}|^2\right).$$

Thanks to its spherical and axial symmetry, $\mathcal{C}[\phi_\alpha]$ becomes a function of μ and ζ (and η) for the function $\phi_\alpha(\eta, \mu, \zeta)$. On the other hand, $\mathcal{C}^S$ is defined for functions of μ and ζ (and η) through $\mathcal{C}$, making use of its axial symmetry:

$$\zeta_i t_i \mathcal{C}^S[\psi_\beta] = \mathcal{C}[\zeta_i t_i \psi_\beta].$$

Once the solutions are obtained, $\Omega_\alpha^{(0)}(\eta)$, $\Theta_\alpha^{(0)}(\eta)$, and $Y_\beta^{(1)}(\eta)$ are obtained as their moment:

$$\Omega_\alpha^{(0)}(\eta) = \langle \phi_\alpha \rangle, \ \Theta_\alpha^{(0)}(\eta) = \frac{2}{3}\langle (\zeta^2 - \frac{3}{2})\phi_\alpha \rangle, \tag{3.3}$$

$$Y_\beta^{(1)}(\eta) = \frac{1}{2}\langle \zeta^2(1-\mu^2)\psi_\beta \rangle, \tag{3.4}$$

where $\langle f \rangle = \int f(\boldsymbol{\xi}) E(|\boldsymbol{\xi}|) d\boldsymbol{\xi}$ with $E(z) = \pi^{-3/2}\exp(-z^2)$.

Our present concern is the case $\alpha = 2, 3, 5$ and $\beta = 4$, for which $(\mathcal{I}_\alpha, g_\alpha)$ and $(\mathcal{I}_\beta^S, g_\beta^S)$ are given as

$$\mathcal{I}_2 = \frac{1}{2}\zeta^2(1-\mu^2)\psi_2(\eta, \mu, \zeta), \tag{3.5a}$$

$$g_2 = 2\mu\zeta \int_0^\infty Y_2^{(1)}(z)dz + \frac{1}{2}\zeta^2(1-3\mu^2)[b_2^{(1)}B(\zeta) + F(\zeta)], \tag{3.5b}$$

$$\mathcal{I}_3 = -\frac{1}{4}\zeta^2(1-\mu^2)\psi_1(\eta, \mu, \zeta), \tag{3.5c}$$

$$g_3 = -\mu\zeta \int_0^\infty Y_1^{(1)}(z)dz - \frac{1}{4}b_1^{(1)}\zeta^2(1-3\mu^2)B(\zeta) - \frac{1}{2}\mu\zeta\left[D_1(\zeta) - \zeta^2(1-2\mu^2)D_2(\zeta)\right], \tag{3.5d}$$

$$\mathcal{I}_5 = 0, \ g_5 = -\frac{1}{3}\zeta^2(1-3\mu^2)B(\zeta), \tag{3.5e}$$

$$\mathcal{I}_4^S = 0, \ g_4^S = -[D_1(\zeta) + \mu^2\zeta^2 D_2(\zeta)]. \tag{3.5f}$$

Here ψ_1 and ψ_2 are respectively the solution of the problem (3.2) with

$$\mathcal{I}_1^S = 0, \ g_1^S = \mu\zeta B(\zeta), \ \mathcal{I}_2^S = 0, \ g_2^S = A(\zeta), \tag{3.6}$$

(the so-called shear-slip and thermal-slip problems [11, 19]), and $(b_1^{(1)}, Y_1^{(1)})$ and $(b_2^{(1)}, Y_2^{(1)})$ are their associated slip coefficient and Knudsen-layer func-

tion, all of which have already been obtained in [15]. Hence $\mathcal{I}_2$ and $\mathcal{I}_3$ in (3.5) indeed decay fast in η. The functions A, B, F, D_1, and D_2 of ζ are familiar solutions of the following integral equations:

$$\begin{aligned}
&\mathcal{L}[\zeta_i A(\zeta)] = -\zeta_i(\zeta^2 - 5/2), \quad \text{subsidiary condition: } \langle \zeta^2 A(\zeta)\rangle = 0,\\
&\mathcal{L}[\zeta_{ij} B(\zeta)] = -2\zeta_{ij}, \quad \mathcal{L}[\zeta_{ij} F(\zeta)] = \zeta_{ij} A(\zeta),\\
&\mathcal{L}[(\zeta_i\delta_{jk} + \zeta_j\delta_{ki} + \zeta_k\delta_{ij})D_1(\zeta) + \zeta_i\zeta_j\zeta_k D_2(\zeta)]\\
&= \gamma_1(\zeta_i\delta_{jk} + \zeta_j\delta_{ki} + \zeta_k\delta_{ij}) - \zeta_i\zeta_j\zeta_k B(\zeta),\\
&\quad \text{subsidiary condition: } \langle 5\zeta^2 D_1(\zeta) + \zeta^4 D_2(\zeta)\rangle = 0,
\end{aligned}$$

where $\mathcal{L}[f] = -\nu(\zeta)f + \mathcal{C}[f]$ and $\zeta_{ij} = \zeta_i\zeta_j - (1/3)\zeta^2\delta_{ij}$.

4. Numerical Analysis

As mentioned at the end of Sec. 2.3, our numerical method is based on the integral form of (3.1) and (3.2).

4.1. Integral formulation

Multiplied by $E(\zeta)$ and integrated with respect to η, both of the problems (3.1) and (3.2) are transformed into

$$\begin{aligned}
\Phi(\eta,\mu,\zeta) =& G(\mu,\zeta)\exp(-\frac{\nu(\zeta)\eta}{\mu\zeta}) + \frac{1}{\mu\zeta}\int_0^\eta C[\Phi](s,\mu,\zeta)\exp(\frac{\nu(\zeta)(s-\eta)}{\mu\zeta})ds\\
&+ \frac{1}{\mu\zeta}\int_0^\eta C[\Psi](s,\mu,\zeta)\exp(\frac{\nu(\zeta)(s-\eta)}{\mu\zeta})ds, \quad (\mu\zeta > 0), \qquad (4.1a)\\
\Phi(\eta,\mu,\zeta) =& \frac{1}{\mu\zeta}\int_\infty^\eta C[\Phi](s,\mu,\zeta)\exp(\frac{\nu(\zeta)(s-\eta)}{\mu\zeta})ds\\
&+ \frac{1}{\mu\zeta}\int_\infty^\eta C[\Psi](s,\mu,\zeta)\exp(\frac{\nu(\zeta)(s-\eta)}{\mu\zeta})ds, \quad (\mu\zeta < 0), \qquad (4.1b)
\end{aligned}$$

with

$$\Phi(\eta,\mu,\zeta) \to 0, \quad \text{as } \eta \to \infty, \qquad (4.1c)$$

$$\Psi(\eta,\mu,\zeta)=\begin{cases}-\dfrac{1}{\mu\zeta}\displaystyle\int_0^\eta I(s,\mu,\zeta)\exp(\frac{\nu(\zeta)(s-\eta)}{\mu\zeta})ds, & (\mu\zeta>0),\\ -\dfrac{1}{\mu\zeta}\displaystyle\int_\infty^\eta I(s,\mu,\zeta)\exp(\frac{\nu(\zeta)(s-\eta)}{\mu\zeta})ds, & (\mu\zeta<0).\end{cases} \tag{4.1d}$$

Here, Φ, C, I, and G should be read as $\Phi=\phi_\alpha E-\Psi$, $C[f]=\mathcal{C}[fE^{-1}]E$, $I=\mathcal{I}_\alpha E$, and $G=(-\sigma_\alpha^{(0)}-c_\alpha^{(0)}\zeta^2+g_\alpha)E$ $(\alpha=2,3,5)$ for problem (3.1), while they should be read as $\Phi=\psi_\beta E-\Psi$, $C[f]=\mathcal{C}^S[fE^{-1}]E$, $I=\mathcal{I}_\beta^S E$, and $G=(-2b_\beta^{(1)}+g_\beta^S)E$ $(\beta=4)$ for problem (3.2). Remember that I decays fast in η, so does Ψ. In the above, the original solution $\phi_\alpha E$ or $\psi_\beta E$ is split into the given part Ψ and unknown part Φ. The equation for Φ is none other than the integral form of the inhomogeneous Boltzmann equation with $C[\Psi]$ being its inhomogeneous term. The conditions (3.1c) and (3.2c) are reduced to (4.1c), because $\Psi\to 0$ as $\eta\to\infty$. The condition (4.1c) is required, otherwise the constants $\sigma_\alpha^{(0)}$, $c_\alpha^{(0)}$, and $b_\beta^{(1)}$ are not determined [1].

Since C is the integral operator, $C[f]$ is mild even if its argument function f is not; thus the factor of steep variation of Φ in (μ,ζ) is picked up explicitly in the above integral form. When $\Phi=\phi_2E-\Psi$ or $\phi_3E-\Psi$, I contains ψ_2 or ψ_1, the solution of the thermal- or shear-slip problem. In the case, the steep variation of Ψ in (μ,ζ) is, at a glance, less clear than that of Φ. However, since ψ_1 and ψ_2 are respectively the solution of (3.2) with (3.6), we can rewrite Ψ in a way that the factor of steep variation is explicit. Namely, in the case of $\Phi=\phi_2E-\Psi$, Ψ can be written as

$$\begin{aligned}\Psi=&-\frac{1-\mu^2}{2\mu}\zeta\Big\{(-2b_2^{(1)}+g_2^S)E(\zeta)\eta\exp(-\frac{\nu(\zeta)\eta}{\mu\zeta})\\ &+\frac{1}{\mu\zeta}\int_0^\eta(\eta-s)C[\psi_2E](s,\mu,\zeta)\exp(\frac{\nu(\zeta)(s-\eta)}{\mu\zeta})ds\Big\},\ (\mu\zeta>0),\end{aligned} \tag{4.2a}$$

$$\Psi=-\frac{1-\mu^2}{2\mu^2}\int_\infty^\eta(\eta-s)C[\psi_2E](s,\mu,\zeta)\exp(\frac{\nu(\zeta)(s-\eta)}{\mu\zeta})ds,\ (\mu\zeta<0), \tag{4.2b}$$

where $C[\psi_2E]=\mathcal{C}^S[\psi_2]E$. In the case of $\Phi=\phi_3E-\Psi$, the above $(-2b_2^{(1)}+g_2^S)$ and ψ_2 are replaced by $-(1/2)(-2b_1^{(1)}+g_1^S)$ and $-(1/2)\psi_1$.

In this way, with the aid of the integral formulation, we can pick up the factor of steep variation in (μ,ζ), which will be advantageous when

the detailed information on the velocity distribution function is required, especially near the boundary.

4.2. Plan of numerical computation

In the computation for solving (4.1), we first prepare the accurate data of $C[\Psi]$ from (4.1d). Then, we abandon the condition (4.1c) and solve (4.1a) and (4.1b) with G being replaced by $\tilde{G} \equiv (-\tilde{\sigma} - \tilde{c}\zeta^2 + g_\alpha)E$ [or $(-2\tilde{b} + g_\beta^S)E$], where $\tilde{\sigma}$ and $\tilde{c}$ (or $\tilde{b}$) are given constants. Let us denote by $\tilde{\Phi}$ the (numerical) solution that is obtained with this process. The difference of $\tilde{\sigma}$ and $\tilde{c}$ (or $\tilde{b}$) from the desired $\sigma_\alpha^{(0)}$ and $c_\alpha^{(0)}$ (or $b_\beta^{(1)}$) results in the asymptote of $\tilde{\Phi}$ such that $\tilde{\Phi} \to (\sigma_\alpha^{(0)} - \tilde{\sigma})E + (c_\alpha^{(0)} - \tilde{c})\zeta^2 E$ [or $2(b_\beta^{(1)} - \tilde{b})E$] as $\eta \to \infty$. This property allows us to determine the constants $\sigma_\alpha^{(0)}$ and $c_\alpha^{(0)}$ (or $b_\beta^{(1)}$) by

$$\sigma_\alpha^{(0)} = \tilde{\sigma} - 2\pi \int_0^\infty \int_{-1}^1 \zeta^2(\zeta^2 - \frac{5}{2})\tilde{\Phi}(\eta \to \infty, \mu, \zeta) d\mu d\zeta,$$
$$c_\alpha^{(0)} = \tilde{c} + \frac{4\pi}{3} \int_0^\infty \int_{-1}^1 \zeta^2(\zeta^2 - \frac{3}{2})\tilde{\Phi}(\eta \to \infty, \mu, \zeta) d\mu d\zeta,$$
$$\Big[\text{or } b_\beta^{(1)} = \tilde{b} + \pi \int_0^\infty \int_{-1}^1 \zeta^4(1 - \mu^2)\tilde{\Phi}(\eta \to \infty, \mu, \zeta) d\mu d\zeta,\Big]$$

and, in turn, to determine Φ by

$$\Phi = \tilde{\Phi} - (\sigma_\alpha^{(0)} - \tilde{\sigma})E - (c_\alpha^{(0)} - \tilde{c})\zeta^2 E. \quad \Big[\text{or } \Phi = \tilde{\Phi} - 2(b_\beta^{(1)} - \tilde{b})E.\Big]$$

For the actual computation, we introduce a finite large distance d from the boundary, beyond which $\tilde{\Phi}$ may be regarded as that at infinity and Ψ may be discarded because of its fast decay in η (see the first paragraph of Sec. 4.1). Then, the problem for $\tilde{\Phi}$ is reduced to

$$\tilde{\Phi}(\eta, \mu, \zeta) = \tilde{G}(\mu, \zeta) \exp(-\frac{\nu(\zeta)\eta}{\mu\zeta}) + \frac{1}{\mu\zeta} \int_0^\eta C[\tilde{\Phi}](s, \mu, \zeta) \exp(\frac{\nu(\zeta)(s - \eta)}{\mu\zeta}) ds$$
$$+ \frac{1}{\mu\zeta} \int_0^\eta C[\Psi](s, \mu, \zeta) \exp(\frac{\nu(\zeta)(s - \eta)}{\mu\zeta}) ds, \quad (\mu\zeta > 0), \qquad (4.3a)$$
$$\tilde{\Phi}(\eta, \mu, \zeta) = \tilde{\Phi}(d, -\mu, \zeta) \exp(\frac{\nu(\zeta)(d - \eta)}{\mu\zeta})$$
$$+ \frac{1}{\mu\zeta} \int_d^\eta C[\tilde{\Phi}](s, \mu, \zeta) \exp(\frac{\nu(\zeta)(s - \eta)}{\mu\zeta}) ds$$

$$+\frac{1}{\mu\zeta}\int_d^\eta C[\Psi](s,\mu,\zeta)\exp(\frac{\nu(\zeta)(s-\eta)}{\mu\zeta})ds, \quad (\mu\zeta<0). \tag{4.3b}$$

Accordingly, ∞'s in (4.1d) or (4.2) may be replaced by d because discarding Ψ beyond d implies discarding I beyond d. All the computations are thus reduced inside a finite region $0 \le \eta \le d$. The occurrence of $\tilde{\Phi}(d,-\mu,\zeta)$ on the right-hand side of (4.3b) comes from that $\tilde{\Phi}(d,\mu,\zeta)=\tilde{\Phi}(d,-\mu,\zeta)$ for d sufficiently large, thanks to its asymptotic form for $\eta\to\infty$. We solve the system (4.3) numerically by iteration for a certain fixed value of d. To be a little more specific, we evaluate $C[\tilde{\Phi}]$ with an initial guess of $\tilde{\Phi}$ and solve (4.3a) first. This gives the data $\tilde{\Phi}(d,-\mu,\zeta)$ in (4.3b), which allows us to solve (4.3b) next. Then we refine the evaluation of $C[\tilde{\Phi}]$ with the updated $\tilde{\Phi}$, and repeat the same process until the numerical solution satisfies a criteria of convergence. The appropriateness of the value of d is judged a posteriori from the result.

4.3. Discretization and some details of numerical method

Thanks to the factor E, $\tilde{\Phi}$ is expected to decay rapidly in ζ. Thus, we truncate the region of ζ at $\zeta=Z(>0)$ for a properly chosen constant Z and restrict the computation in the region $-1\le\mu\le 1$, $0\le\zeta\le Z$, and $0\le\eta\le d$. Justification of the chosen value of Z is made a posteriori again from the resulting solution. Non-uniform discretization is made in order to capture the possible steep variation of $\tilde{\Phi}$. The grid in molecular velocity space (μ,ζ) is arranged two-fold: one is the grid for capturing the milder function $C[\tilde{\Phi}]$ (and $C[\Psi]$), while the other is that for capturing $\tilde{\Phi}$ (and Ψ) to compute $C[\tilde{\Phi}]$ (and $C[\Psi]$) enough accurately. The latter grid should be finer than the former. In the standard grid system, namely (S1,M1) in the Appendix B.1, we set $Z=5.0$ and $d=44.46$, and arrange 251 grid points in η space; the two-fold grid in μ-ζ space consists of 257×141 and 449×161 points. More details are found in the Appendix B.1.

For the spatial coordinate η and related integration, we arrange $2N_\eta+1$ grid points, say $\eta^{(i)}$ $(i=0,1,\dots,2N_\eta)$, in the region $0\le\eta\le d$:

$$0=\eta^{(0)}<\eta^{(1)}<\cdots<\eta^{(2N_\eta)}=d. \tag{4.4}$$

The functions $\tilde{\Phi}$ and Ψ are evaluated on these points. In carrying out the integration with respect to s in (4.3), $C[\tilde{\Phi}]$ and $C[\Psi]$ are interpolated with a

piecewise quadratic function from their data on the grid points $\{\eta^{(i)}\}$.[1] The related integrals are commonly expressed as

$$T[F](\eta,\mu,\zeta)=\begin{cases}\dfrac{1}{\mu\zeta}\displaystyle\int_0^{\eta} C[F](s,\mu,\zeta)\exp(\frac{\nu(\zeta)(s-\eta)}{\mu\zeta})ds, & (\mu\zeta>0),\\ \dfrac{1}{\mu\zeta}\displaystyle\int_d^{\eta} C[F](s,\mu,\zeta)\exp(\frac{\nu(\zeta)(s-\eta)}{\mu\zeta})ds, & (\mu\zeta<0),\end{cases} \tag{4.5}$$

with $F=\tilde{\Phi}$ or Ψ. By the piecewise quadratic interpolation for $C[F]$ in s, $T[F]$ is computed as

$$T[F](\eta^{(i)},\mu,\zeta)=\sum_{r=0}^{2N_\eta} S_{i,r}(\mu,\zeta)C[F](\eta^{(r)},\mu,\zeta), \tag{4.6}$$

with

$$S_{i,r}(\mu,\zeta)=\begin{cases}\dfrac{1}{\mu\zeta}\displaystyle\int_0^{\eta^{(i)}} Y_r^{\eta}(s)\exp(\frac{\nu(\zeta)(s-\eta^{(i)})}{\mu\zeta})ds, & (\mu\zeta>0),\\ \dfrac{1}{\mu\zeta}\displaystyle\int_d^{\eta^{(i)}} Y_r^{\eta}(s)\exp(\frac{\nu(\zeta)(s-\eta^{(i)})}{\mu\zeta})ds, & (\mu\zeta<0),\end{cases} \tag{4.7}$$

where Y's are the following locally defined piecewise quadratic functions:

$$Y_{2r}^{z}(y)=\begin{cases}\frac{(y-z^{(2r+2)})(y-z^{(2r+1)})}{(z^{(2r)}-z^{(2r+2)})(z^{(2r)}-z^{(2r+1)})}, & (z^{(2r)}<y<z^{(2r+2)}),\\ \frac{(y-z^{(2r-2)})(y-z^{(2r-1)})}{(z^{(2r)}-z^{(2r-2)})(z^{(2r)}-z^{(2r-1)})}, & (z^{(2r-2)}<y<z^{(2r)}),\\ 0, \quad \text{otherwise},\end{cases} \tag{4.8a}$$

$$Y_{2r+1}^{z}(y)=\begin{cases}\frac{(y-z^{(2r)})(y-z^{(2r+2)})}{(z^{(2r+1)}-z^{(2r)})(z^{(2r+1)}-z^{(2r+2)})}, & (z^{(2r)}<y<z^{(2r+2)}),\\ 0, \quad \text{otherwise}.\end{cases} \tag{4.8b}$$

The functional form of $S_{i,r}$ can be obtained explicitly, which enables us to perform delicate analyses with numerically obtained data. With the data $C[\tilde{\Phi}](\eta^{(i)},\mu,\zeta)$ and $C[\Psi](\eta^{(i)},\mu,\zeta)$, we can obtain $\tilde{\Phi}$ on the spatial grid points $\{\eta^{(i)}\}$, essentially by the simple summation (4.6).[2]

[1]The quadratic interpolation cannot capture a possible logarithmic divergence of the gradient of $\tilde{\Phi}$ with respect to $\mu\zeta$ on the boundary for $\mu\zeta=0_-$, which is discussed in [24]. However, it does capture the logarithmic divergence of the gradient of the Knudsen-layer functions with respect to η (see [24]), thanks to the integral formulation. See the last paragraph of Sec. 5.2.

[2]In computing Ψ, the integrations in (4.2) with ∞ being replaced with d are performed in the same way. In the case, the piecewise quadratic interpolation is applied to $C[\psi_2 E]$.

As already mentioned in the first paragraph of this section, we prepare the two-fold grid system for molecular velocity space. As the primary grid, we arrange $(4N_\mu+1)\times(2N_\zeta+1)$ points, say $(\mu^{(j)},\zeta^{(k)})$ $(j=-2N_\mu,\dots,2N_\mu;$ $k=0,\dots,2N_\zeta)$ in the region $-1\le\mu\le 1$ and $0\le\zeta\le Z$:

$$\begin{aligned}
&0=\mu^{(0)}<\mu^{(1)}<\cdots<\mu^{(2N_\mu-1)}<\mu^{(2N_\mu)}=1,\\
&\mu^{(-j)}=-\mu^{(j)},\ (1\le j\le 2N_\mu),\\
&0=\zeta^{(0)}<\zeta^{(1)}<\cdots<\zeta^{(2N_\zeta)}=Z,
\end{aligned}$$

which have the enough resolution for the mild function $C[F]$. Then $C[F](\eta^{(i)},$ $\mu,\zeta)$ is recovered accurately for any μ and ζ by the piecewise quadratic interpolation of $C[F]_{(i,j,k)}\equiv C[F](\eta^{(i)},\mu^{(j)},\zeta^{(k)})$. Hence $\tilde{\Phi}(\eta^{(i)},\mu,\zeta)$ is obtained by (4.3) accurately for any μ and ζ. This applies also to $\Psi(\eta^{(i)},\mu,\zeta)$.[3]

In order to obtain $C[F]_{(i,j,k)}$, we use the *numerical kernel method* that was first proposed in [20]. In this method, the argument function F is approximated by interpolation from the discretized data of F, so that a grid finer than the primary one is required for achieving the enough resolution of F. Therefore, as the secondary grid, we prepare $(4N_M+1)\times(2N_\xi+1)$ points in μ-ζ space, say $(M^{(l)},\xi^{(m)})$ $(l=-2N_M,\dots,2N_M;\ m=0,\dots,2N_\xi)$:

$$\begin{aligned}
&0=M^{(0)}<M^{(1)}<\cdots<M^{(2N_M-1)}<M^{(2N_M)}=1,\\
&M^{(-l)}=-M^{(l)},\ (1\le l\le 2N_M),\\
&0=\xi^{(0)}<\xi^{(1)}<\cdots<\xi^{(2N_\xi)}=Z.
\end{aligned}$$

Note that $N_M>N_\mu$ and $N_\xi>N_\zeta$ and that $F(\eta^{(i)},M^{(l)},\xi^{(m)})$ (for short, to be denoted by $F_{[i,l,m]}$ below) on the secondary grid is readily obtained as explained in the previous paragraph. In the present work, we adopt the piecewise quadratic interpolation for F:

$$F(\eta^{(i)},M,\xi)=\sum_{m=0}^{2N_\xi}\sum_{l=0}^{2N_M}[F_{[i,l,m]}B^{+}_{l,m}(M,\xi)+F_{[i,-l,m]}B^{-}_{-l,m}(M,\xi)],\quad(4.9a)$$

[3]The primary grid should also have the enough resolution for $C[\psi_1 E]$ and $C[\psi_2 E]$ in (4.2) for the accurate computation of Ψ.

with

$$B^{\pm}_{l,m}(M,\xi) = Y_l^M(M)\chi[0,1](\pm M)Y_m^{\xi}(\xi)\chi[0,Z](\xi), \tag{4.9b}$$

$$\chi[a,b](y) = \begin{cases} 1 & \text{for } a \le y \le b, \\ 0 & \text{otherwise,} \end{cases} \tag{4.9c}$$

and compute $C[F]_{(i,j,k)}$ as

$$C[F]_{(i,j,k)} = \sum_{m=0}^{2N_\xi} \sum_{l=0}^{2N_M} (C^{+}_{j,k,l,m} F_{[i,l,m]} + C^{-}_{j,k,-l,m} F_{[i,-l,m]}), \tag{4.10a}$$

$$C^{\pm}_{j,k,l,m} = C[B^{\pm}_{l,m}](\mu^{(j)}, \zeta^{(k)}). \tag{4.10b}$$

Note that, as the arguments of functions in (4.9), we use the integration variables $\xi(\equiv |\boldsymbol{\xi}|)$ and $M(\equiv \xi_i n_i/\xi)$, in place of ζ and μ, coming from $\boldsymbol{\xi}$ in the definition of $\mathcal{C}$ or C. The factor $\chi[0,1](\pm M)$ is included in (4.9b) to reflect that F can be discontinuous at $M = 0$ on the boundary $\eta = 0$, as will be shown in Sec. 5.1. Hence, $F_{[i,l,m]}$ and $F_{[i,-l,m]}$ in (4.9a) [and (4.10a) soon below] should be considered different from each other, when $i = l = 0$. Note that $B^{\pm}_{l,m}$ vanishes for $l \lesseqgtr 0$ and that the discrimination between $B^{+}_{l,m}$ and $B^{-}_{l,m}$ is effective when $l = 0$. Accordingly, $C^{\pm}_{j,k,l,m}$ corresponds to the integral kernel for the half-range of integration $M \gtreqless 0$, and $C^{\pm}_{j,k,l,m}$ vanishes for $l \lesseqgtr 0$. The computation of $C^{\pm}_{j,k,l,m}$, i.e., (4.10b), can be performed beforehand, independent of the iteration for solving (4.3). Incidentally, the integrations for this computation require careful treatments and some transformations to get rid of the singularity in the kernel k_1. However, we omit all the details on this issue; the interested reader is referred to [15, 20].

Here are two remarks. (i) As is clear from its form, the collision kernel $k_1(\boldsymbol{\zeta},\boldsymbol{\xi}) - k_2(\boldsymbol{\zeta},\boldsymbol{\xi})$ is invariant under the transformation $(\boldsymbol{\zeta},\boldsymbol{\xi}) \to (-\boldsymbol{\zeta},-\boldsymbol{\xi})$. The symmetric arrangement of grid points in μ with respect to $\mu = 0$ enables the present numerical kernel $C^{\pm}_{j,k,l,m}$ to inherit this property, giving the relation $C^{-}_{j,k,l,m} = C^{+}_{-j,k,-l,m}$. This reduces the required memory capacity into half. (ii) If we have adopted a finite-difference method, we would need the secondary grid for the whole numerical solution process, which implies

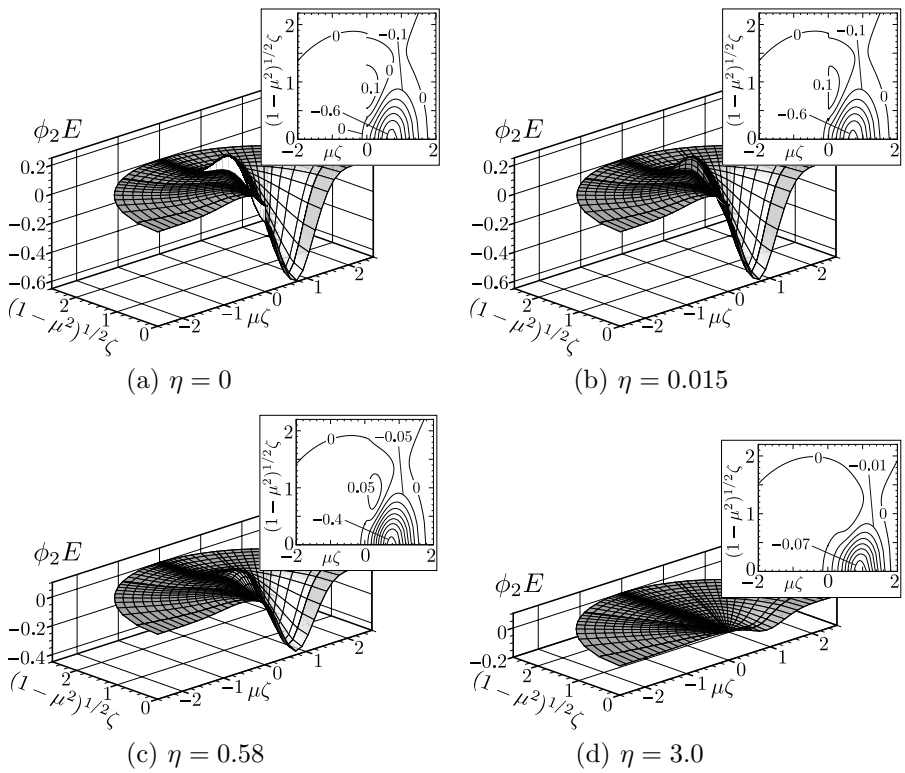

Figure 5.1: $\phi_2 E$ and its contour plots at four spatial points. (a) $\eta = 0$, (b) $\eta = 0.015$, (c) $\eta = 0.58$, and (d) $\eta = 3.0$. In the contour plots, the curves are drawn with the intervals 0.1 in (a) and (b), 0.05 in (c), and 0.01 in (d). The white vertical surface at $\mu\zeta = 0$ in (a) shows the discontinuity.

the size of the numerical kernel to be of $(N_M \times N_\xi)^2$. The present approach economizes again the memory capacity by a factor of $(N_\mu \times N_\zeta)/(N_M \times N_\xi)$.

5. Numerical Results

The results in the present section are obtained by the standard grid (S1,M1), unless otherwise stated.

5.1. Velocity distribution function

As illustrative examples, we show $\phi_2 E$ and $\phi_5 E$ at four spatial points $\eta = 0$, 0.015, 0.58, 3.0 in Figs. 5.1 and 5.2. The former is the case with

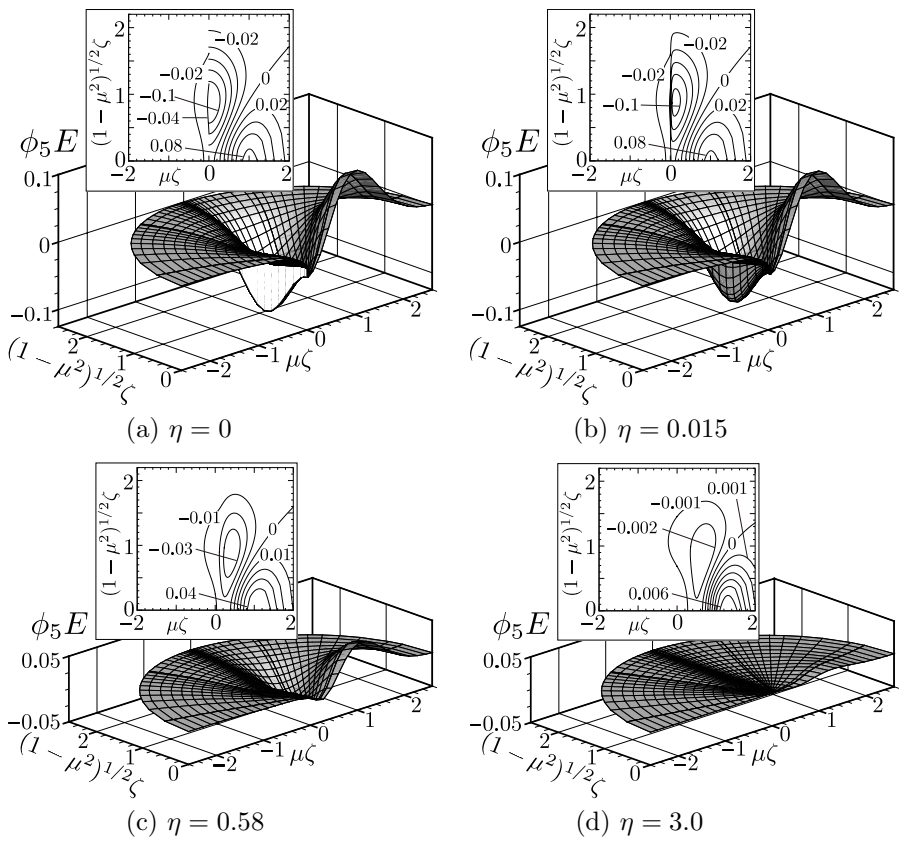

(a) $\eta = 0$ (b) $\eta = 0.015$

(c) $\eta = 0.58$ (d) $\eta = 3.0$

Figure 5.2: $\phi_5 E$ and its contour plots at four spatial points. (a) $\eta = 0$, (b) $\eta = 0.015$, (c) $\eta = 0.58$, and (d) $\eta = 3.0$. In the contour plots the curves are drawn with the intervals 0.02 in (a) and (b), 0.01 in (c), and 0.001 in (d). The white vertical surface at $\mu\zeta = 0$ in (a) shows the discontinuity.

nonzero Ψ in (4.1), while the latter is the case without it (or $\Psi = 0$). On the boundary $\eta = 0$, the discontinuity is commonly observed along the line $\mu\zeta = 0$. This line corresponds to the direction of molecular velocity that is tangential to the boundary. [Remind that the positive (or negative) $\mu\zeta$ corresponds to the velocity of molecules outgoing from (or incoming onto) the boundary.] The discontinuity vanishes immediately away from the boundary with keeping the other part almost unchanged. Accordingly, a continuous but steep variation part in the molecular velocity space appears near the boundary [see the panel (b) in both figures]. Such a local deformation can be understood by that the molecules coming from the boundary with small normal velocity ($\mu\zeta \sim 0$) would travel a long distance in the tangential

Table 5.1: Slip/jump coefficients. The data in [25] obtained by the use of the symmetry relation are also shown for comparisons.

	$c_2^{(0)}$	$c_3^{(0)}$	$c_5^{(0)}$	$b_4^{(1)}$
Present results	-0.4993	0.00874	0.45957	-0.90393
Symmetry relation [25]	-0.4992	0.0087	0.4596	-0.9039

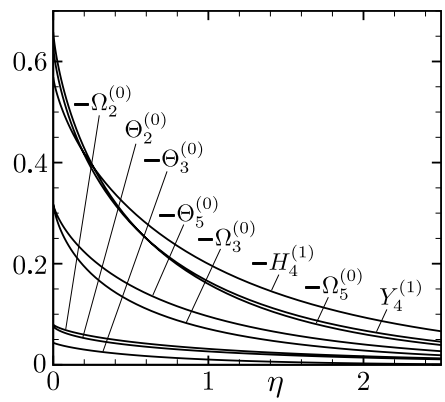

Figure 5.3: Knudsen-layer functions.

direction before reaching the position of interest, thus more likely collide with others first to deform the part $\mu\zeta \sim 0$. As going away from the boundary, the distribution becomes milder and tends to vanish with keeping non-similar form between the positive and the negative $\mu\zeta$ part. The qualitative feature described above is common in both figures, irrespective of whether or not the inhomogeneous term appears in the problem (4.1).

5.2. Slip/jump coefficient and Knudsen-layer function

Slip/jump coefficients are shown in Table 5.1. The data in [25], which are obtained from the information about the first-order Knudsen layer by the theory of symmetry relation [21], are also shown for comparisons. Excellent agreement ensures the consistency of the present results to the theory.

The Knudsen-layer functions Ω's, Θ's, $Y_4^{(1)}$, and $H_4^{(1)}$ are shown in Fig. 5.3 and Table 5.2 (see Appendix A for $H_4^{(1)}$). Corresponding to the behavior of the velocity distribution functions in η, they decay fast as $\eta \to \infty$, mostly monotonically except for $\Theta_3^{(0)}$ and $\Theta_5^{(0)}$ (see Table 5.2). From the table, the 90% thickness of the Knudsen layer is seen to be about $3 \sim 3.5$

Table 5.2: Knudsen-layer functions.

η	$-\Omega_2^{(0)}$	$\Theta_2^{(0)}$	$-\Omega_3^{(0)}$	$-\Theta_3^{(0)}$	$-\Omega_5^{(0)}$	$-\Theta_5^{(0)}$	$Y_4^{(1)}$	$-H_4^{(1)}$
0.00000	0.07965	0.07610	0.31803	0.04368	0.65823	0.31749	0.62894	0.56938
0.02348	0.07508	0.07019	0.28692	0.04108	0.60555	0.29707	0.58003	0.53685
0.05165	0.07153	0.06590	0.26406	0.03872	0.56413	0.28044	0.54166	0.51032
0.09881	0.06693	0.06064	0.23601	0.03547	0.51105	0.25858	0.49254	0.47522
0.15009	0.06290	0.05623	0.21276	0.03253	0.46540	0.23928	0.45030	0.44399
0.19315	0.05999	0.05316	0.19673	0.03038	0.43311	0.22536	0.42042	0.42128
0.30336	0.05380	0.04689	0.16463	0.02578	0.36657	0.19589	0.35876	0.37265
0.40911	0.04897	0.04220	0.14146	0.02224	0.31708	0.17323	0.31279	0.33467
0.58327	0.04252	0.03618	0.11301	0.01763	0.25470	0.14363	0.25459	0.28411
0.79673	0.03628	0.03059	0.08822	0.01340	0.19900	0.11603	0.20221	0.23582
0.98271	0.03187	0.02674	0.07228	0.01059	0.16263	0.09728	0.16769	0.20222
1.19037	0.02776	0.02323	0.05863	0.00814	0.13118	0.08051	0.13752	0.17148
1.41884	0.02400	0.02007	0.04715	0.00606	0.10458	0.06582	0.11167	0.14392
1.58214	0.02170	0.01814	0.04061	0.00488	0.08938	0.05719	0.09672	0.12738
1.84260	0.01856	0.01554	0.03230	0.00340	0.07008	0.04592	0.07747	0.10530
2.02594	0.01667	0.01399	0.02764	0.00259	0.05931	0.03945	0.06657	0.09234
2.51495	0.01263	0.01067	0.01860	0.00109	0.03855	0.02654	0.04506	0.06560
3.04221	0.00947	0.00807	0.01245	0.00019	0.02469	0.01748	0.03014	0.04586
3.48717	0.00748	0.00642	0.00901	-0.00022	0.01716	0.01236	0.02171	0.03412
4.06758	0.00554	0.00481	0.00603	-0.00049	0.01082	0.00790	0.01433	0.02336
4.91724	0.00362	0.00319	0.00345	-0.00059	0.00565	0.00412	0.00795	0.01356
6.06059	0.00207	0.00186	0.00172	-0.00050	0.00245	0.00171	0.00370	0.00662
8.07087	0.00081	0.00074	0.00056	-0.00028	0.00063	0.00034	0.00101	0.00193
10.06348	0.00032	0.00030	0.00020	-0.00013	0.00018	0.00005	0.00029	0.00058
13.81166	0.00006	0.00006	0.00003	-0.00003	0.00002	-0.00001	0.00003	0.00006
15.00856	0.00004	0.00003	0.00002	-0.00002	0.00001	-0.00001	0.00002	0.00003
20.05147	0.00000	0.00000	0.00000	0.00000	0.00000	0.00000	0.00000	0.00000
25.14669	0.00000	0.00000	0.00000	0.00000	0.00000	0.00000	0.00000	0.00000
$\eta \ln \eta^*$	0.0546	0.0809	0.405	0.0153	0.584	0.207	0.546	0.338

* The Knudsen-layer function has the singularity $\eta \ln \eta$ at $\eta = 0$. Its coefficient is shown in this row.

for $\Omega_2^{(0)}$ and $\Theta_2^{(0)}$, about $2.5 \sim 3$ for $H_4^{(1)}$, and about $1.5 \sim 2$ for the others, measured in η, meaning about three mean-free-path thickness at most.

One interesting observation could be on the data of $c_2^{(0)}$, $\Omega_2^{(0)}$, and $\Theta_2^{(0)}$, as well as on the corresponding distribution function ϕ_2. In the case of the BGK model under the diffuse reflection boundary condition, the former three all degenerate (or vanish) (see, e.g., [19]) in spite of the fact that ϕ_2 itself does not vanish [see (3.5a) and (3.5b)]. The present results demonstrate that such a complete cancellation is not expected and the missing temperature jump and associated Knudsen layer indeed come out in general.

It is known that the Knudsen-layer function has the singularity $\eta \ln \eta$ on the boundary $\eta = 0$, which is another interest of the present work. This singularity that occurs on a plane boundary was first found in the study of the Rayleigh problem [16] on the basis of the BGK model. The same singularity has recently been confirmed to occur on the basis of the Boltzmann equation for hard-sphere molecules [24]. By the least-squares fitting of the curve $a + b\,\eta \ln \eta + c\eta$ to the numerical data near the boundary, we

determine the coefficient b of the singularity $\eta \ln \eta$ for each Knudsen-layer function. The results are shown in the last row of Table 5.2. Incidentally, determining these coefficients is really challenging. Indeed, we could not get them by the finite-difference approach, even with the same computational size as [27]. The integral formulation enabled us to do it (see footnote 1).

Acknowledgments

The present work is supported in part by KAKENHI from JSPS (Nos. 23360083 and 13J01011). The authors thank Professor Kazuo Aoki, Kyoto University, for his interest and encouragement.

Appendix A. Stress and Heat Flow

The stress tensor and heat-flow vector are also familiar fluid-dynamic quantities that become necessary, most typically, in computing the momentum and energy exchange with the body surface. Denoting the former by $p_0(\delta_{ij}+P_{ij})$ and the latter by $p_0(2RT_0)^{1/2}Q_i$, their Hilbert part and Knudsen-layer correction up to the second order in ε are summarized as follows:

$$P_{ij\mathrm{H}m} = P_{\mathrm{H}m}\delta_{ij} - \gamma_1 \overline{\frac{\partial u_{i\mathrm{H}m-1}}{\partial x_j}} + \frac{1}{2}\gamma_3 \overline{\frac{\partial^2 \tau_{\mathrm{H}m-2}}{\partial x_i \partial x_j}}, \ (m = 0, 1, 2), \tag{A.1a}$$

$$Q_{i\mathrm{H}m} = -\frac{5}{4}\gamma_2 \frac{\partial \tau_{\mathrm{H}m-1}}{\partial x_i} + \frac{1}{2}\gamma_3 \frac{\partial^2 u_{i\mathrm{H}m-2}}{\partial x_j^2}, \ (m = 0, 1, 2), \tag{A.1b}$$

and

$$P_{ij\mathrm{K}m} = \frac{3}{2}\frac{\partial \tau_{\mathrm{H}m-1}}{\partial x_k} n_k(\delta_{ij} - n_i n_j)[\Omega_1^{(0)}(\eta) + \Theta_1^{(0)}(\eta)], \ (m = 0, 1), \tag{A.2a}$$

$$P_{ij\mathrm{K}2} n_i n_j = -3\bar{\kappa}\frac{\partial \tau_{\mathrm{H}0}}{\partial x_i} n_i \int_\eta^\infty [\Omega_1^{(0)}(z) + \Theta_1^{(0)}(z)]dz, \tag{A.2b}$$

$$P_{ij\mathrm{K}2} n_i t_j = \frac{3}{2}\Big(\frac{\partial^2 \tau_{\mathrm{H}0}}{\partial x_i \partial x_j} n_i t_j + \kappa_{ij} t_j \frac{\partial \tau_{\mathrm{H}0}}{\partial x_i}\Big) \int_\eta^\infty [\Omega_1^{(0)}(z) + \Theta_1^{(0)}(z)]dz, \tag{A.2c}$$

$$\begin{aligned} Q_{i\mathrm{K}m} t_i =& \overline{\frac{\partial u_{i\mathrm{H}m-1}}{\partial x_j}} n_i t_j H_1^{(1)}(\eta) + \frac{\partial \tau_{\mathrm{H}m-1}}{\partial x_i} t_i H_2^{(1)}(\eta) \\ &+ \frac{\partial^2 \tau_{\mathrm{H}m-2}}{\partial x_i \partial x_j} n_i t_j H_3^{(1)}(\eta) + \frac{\partial}{\partial x_i} \overline{\frac{\partial u_{j\mathrm{H}m-2}}{\partial x_k}} n_i n_j t_k H_4^{(1)}(\eta) \end{aligned}$$

$$+\bar{\kappa}\overline{\frac{\partial u_{i\mathrm{H}m-2}}{\partial x_j}}n_it_jH_5^{(1)}(\eta)+\kappa_{ij}\overline{\frac{\partial u_{j\mathrm{H}m-2}}{\partial x_k}}n_kt_iH_6^{(1)}(\eta)$$

$$+\kappa_{ij}t_j\frac{\partial \tau_{\mathrm{H}m-2}}{\partial x_i}H_7^{(1)}(\eta)+\bar{\kappa}\frac{\partial \tau_{\mathrm{H}m-2}}{\partial x_i}t_iH_8^{(1)}(\eta),\ (m=0,1,2), \quad \text{(A.2d)}$$

$$Q_{i\mathrm{K}m}n_i=\left[\frac{\partial^2\tau_{\mathrm{H}m-2}}{\partial x_i\partial x_j}(\delta_{ij}-n_in_j)-2\bar{\kappa}\frac{\partial \tau_{\mathrm{H}m-2}}{\partial x_i}n_i\right]\int_\eta^\infty H_2^{(1)}(z)dz$$

$$-\frac{1}{2}\frac{\partial}{\partial x_i}\overline{\frac{\partial u_{j\mathrm{H}m-2}}{\partial x_k}}n_in_jn_k\int_\eta^\infty H_1^{(1)}(z)dz,\ (m=0,1,2). \quad \text{(A.2e)}$$

Here the quantities with the subscript H in (A.2) denote their value on the boundary. The functions $H_1^{(1)}$, $H_2^{(1)}$, and $H_3^{(1)}$ have already been obtained in [15, 14]. The present work newly provides the data of $H_4^{(1)}$, which are included in Table 5.2 and Fig. 5.3.

B. Data of Computations

B.1. Grid system

Grid points for spatial coordinate η are arranged in the interval $[0,d]$ as

$$\eta^{(i)}=-20\ln(1-0.7p^{(i)})+10^{-4}\frac{i}{2N}, \quad \text{(B.1a)}$$

$$p^{(i)}=\frac{26(i/2N)^4}{1+25(i/2N)^3},\quad (i=0,1,\dots,2N_\eta). \quad \text{(B.1b)}$$

The parameters N and N_η and the upper bound $d(=\eta^{(2N_\eta)})$ for the grids S1, S2, and S3 are as follows: $(N,N_\eta,d)=(100,125,44.46)$ for S1, $(N,N_\eta,d)=(150,188,44.94)$ for S2, and $(N,N_\eta,d)=(100,130,53.04)$ for S3.

As to the μ and ζ spaces, subintervals $(0,\mu_{\mathrm{I}}]$, $(\mu_{\mathrm{I}},\mu_{\mathrm{II}}]$, and $(\mu_{\mathrm{II}},1]$ in μ and $[0,\zeta_{\mathrm{I}}]$, $(\zeta_{\mathrm{I}},\zeta_{\mathrm{II}}]$, and $(\zeta_{\mathrm{II}},Z]$ in ζ are conveniently introduced for the easy control of grid points near $\mu=0$ and $\zeta=0$; the grid points are arranged as

$$\mu^{(j)}=\begin{cases}0, & (j=0),\\ 1-\tanh\left(\frac{\pi}{2}\sinh(u^{(j)})\right), & (j=1,\dots,2N_{\mathrm{II}}),\\ \left(\mu_{\mathrm{II}}^{1/3}+(1-\mu_{\mathrm{II}}^{1/3})\frac{j-2N_{\mathrm{II}}}{2N_\mu-2N_{\mathrm{II}}}\right)^3, & (j=2N_{\mathrm{II}}+1,\dots,2N_\mu),\\ -\mu^{(-j)}, & (j=-2N_\mu,\dots,-1),\end{cases} \quad \text{(B.2a)}$$

Table B.3: Grid parameters for μ-ζ space.

	Common		Primary grid					Secondary grid				
	$\mu_{\rm I}$	$\mu_{\rm II}$	$N_{\rm I}$	$N_{\rm II}$	N_μ		w	$N_{\rm I}$	$N_{\rm II}$	N_M		w
	$\zeta_{\rm I}$	r	$\mathcal{N}_{\rm I}$	$\mathcal{N}_{\rm II}$	N_ζ	$\mathcal{N}$	W	$\mathcal{N}_{\rm I}$	$\mathcal{N}_{\rm II}$	N_ξ	$\mathcal{N}$	W
Grid	Z	$\zeta_{\rm II}$	$\mu^{(1)}$		$\zeta^{(1)}$			$M^{(1)}$		$\xi^{(1)}$		
M1	10^{-4}	1/125	0	16	64		-	48	64	112		1
	10^{-4}	1/10	0	16	70	70	-	10	26	80	80	1
	5.0	0.36	1.2×10^{-4}		1.6×10^{-4}			2.4×10^{-10}		5.1×10^{-10}		
M2	10^{-4}	1/125	0	16	64		-	64	80	128		1
	10^{-4}	1/10	0	16	70	70	-	10	26	80	80	1
	5.0	0.36	1.2×10^{-4}		1.6×10^{-4}			2.3×10^{-10}		5.1×10^{-10}		
M3	10^{-4}	1/125	0	16	64		-	48	64	112		1
	10^{-4}	1/10	0	22	94	94	-	14	36	108	108	1
	5.0	0.36	1.2×10^{-4}		1.4×10^{-4}			2.4×10^{-10}		3.9×10^{-10}		
M4	10^{-4}	1/125	0	22	86		-	48	70	134		1
	10^{-4}	1/10	0	16	70	70	-	10	26	80	80	1
	5.0	0.36	1.1×10^{-4}		1.6×10^{-4}			2.4×10^{-10}		5.1×10^{-10}		
M5	10^{-4}	1/125	5	21	69		5/24	53	69	117		53/48
	10^{-4}	1/10	5	21	75	75	5/24	12	28	82	82	12/10
	5.0	0.36	1.8×10^{-5}		1.8×10^{-5}			3.1×10^{-11}		9.3×10^{-12}		
M6	10^{-4}	1/125	0	16	64		-	48	64	112		1
	10^{-4}	1/10	0	16	73	70	-	10	26	83	80	1
	5.8	0.36	1.2×10^{-4}		1.6×10^{-4}			2.4×10^{-10}		5.1×10^{-10}		
M7	10^{-4}	1/125	0	12	48		-	36	48	84		1
	10^{-4}	1/10	0	12	48	48	-	7	19	55	55	1
	5.0	0.36	1.3×10^{-4}		1.8×10^{-4}			2.6×10^{-10}		7.5×10^{-10}		

with

$$u^{(j)} = \begin{cases} (2.69 - u_{\rm I})w(1 - \frac{j}{2N_{\rm I}}) + u_{\rm I}, \ (j = 1, \ldots, 2N_{\rm I}), \\ (1 - \frac{j-2N_{\rm I}}{2N_{\rm II}-2N_{\rm I}})u_{\rm I} + \frac{j-2N_{\rm I}}{2N_{\rm II}-2N_{\rm I}}u_{\rm II}, \ (j = 2N_{\rm I}+1, \ldots, 2N_{\rm II}), \end{cases} \tag{B.2b}$$

$$u_{\rm I,II} = \sinh^{-1}\left(\frac{2}{\pi}\tanh^{-1}(1 - \mu_{\rm I,II})\right), \tag{B.2c}$$

and

$$\zeta^{(k)} = \begin{cases} 0, \ (k = 0), \\ 1 - \tanh\left(\frac{\pi}{2}\sinh(v^{(k)})\right), \ (k = 1, \ldots, 2\mathcal{N}_{\rm II}), \\ 3.6v^{(k)} + 1.4(v^{(k)})^8, \ (k = 2\mathcal{N}_{\rm II}+1, \ldots, 2N_\zeta), \end{cases} \tag{B.3a}$$

with

$$v^{(k)} = \begin{cases} (2.69 - v_{\rm I})W(1 - \frac{k}{2\mathcal{N}_{\rm I}}) + v_{\rm I}, \ (k = 1, \ldots, 2\mathcal{N}_{\rm I}), \\ v_{\rm I}(1 - \frac{k-2\mathcal{N}_{\rm I}}{2\mathcal{N}_{\rm II}-2\mathcal{N}_{\rm I}}) + v_{\rm II}\frac{k-2\mathcal{N}_{\rm I}}{2\mathcal{N}_{\rm II}-2\mathcal{N}_{\rm I}}, \ (k = 2\mathcal{N}_{\rm I}+1, \ldots, 2\mathcal{N}_{\rm II}), \\ r + (1-r)\frac{k-2\mathcal{N}_{\rm II}}{2\mathcal{N}-2\mathcal{N}_{\rm II}}, \ (k = 2\mathcal{N}_{\rm II}+1, \ldots, 2N_\zeta), \end{cases} \tag{B.3b}$$

Table B.4: Slip/jump coefficients $c_2^{(0)}$, $c_3^{(0)}$, $c_5^{(0)}$, and $b_4^{(1)}$ obtained by different grids.

Grid	$c_2^{(0)}$	$c_3^{(0)}$	$c_5^{(0)}$	$b_4^{(1)}$
(S1,M1)	-0.4992519	0.0087359	0.4595723	-0.9039300
(S1,M2)	-0.4992519	0.0087359	0.4595723	-0.9039300
(S1,M3)	-0.4992695	0.0087344	0.4595690	-0.9039293
(S1,M4)	-0.4992535	0.0087370	0.4595721	-0.9039303
(S1,M5)	-0.4992519	0.0087359	0.4595723	-0.9039300
(S1,M6)	-0.4992532	0.0087358	0.4595722	-0.9039301
(S1,M7)	-0.4991404	0.0087413	0.4595929	-0.9039335
(S2,M1)	-0.4992531	0.0087359	0.4595723	-0.9039288
(S3,M1)	-0.4992519	0.0087359	0.4595723	-0.9039300

$$v_{\mathrm{I,II}} = \sinh^{-1}\left(\frac{2}{\pi}\tanh^{-1}(1-\zeta_{\mathrm{I,II}})\right), \quad \zeta_{\mathrm{II}} = 3.6r + 1.4r^8. \tag{B.3c}$$

Note that $\mu^{(\pm 2N_{\mathrm{I}})} = \pm\mu_{\mathrm{I}}$, $\mu^{(\pm 2N_{\mathrm{II}})} = \pm\mu_{\mathrm{II}}$, $\mu^{(\pm 2N_\mu)} = \pm 1$, $\zeta^{(2\mathcal{N}_{\mathrm{I}})} = \zeta_{\mathrm{I}}$, $\zeta^{(2\mathcal{N}_{\mathrm{II}})} = \zeta_{\mathrm{II}}$, and $\zeta^{(2N_\zeta)} = Z$. In (B.2) and (B.3), the primary grid is supposed. For the secondary grid, $\mu^{(j)}$, N_μ, $\zeta^{(k)}$, and N_ζ should be replaced by $M^{(j)}$, N_M, $\xi^{(k)}$, and N_ξ, respectively. Although the common notation is used for $N_{\mathrm{I,II}}$, w, $\mathcal{N}_{\mathrm{I,II}}$, $\mathcal{N}$, and W, they may take different values between the primary and the secondary grid. The values of grid parameters for the μ and ζ spaces, as well as the resulting values of Z, ζ_{II}, $\mu^{(1)}$, $\zeta^{(1)}$, $M^{(1)}$, and $\xi^{(1)}$, are summarized in Table B.3.

B.2. Measure of accuracy

The truncation of the ζ and η spaces is justified by checking the ratios $F(d,\cdot,\cdot)/F_{\max}$ and $F(\cdot,\cdot,Z)/F_{\max}$, where $F = |\phi_2 E|$, $|\phi_3 E|$, $|\phi_5 E|$, and $|\psi_4 E|$ and $F_{\max}$ is the respective maximum of F over the all grid points. For the standard grid (S1,M1) computation, the former and the latter are respectively less than 8.9×10^{-11} and 1.4×10^{-9}. The velocity distribution functions have decayed sufficiently at the truncated point.

The grid dependence of the computed slip/jump coefficients is shown in Table B.4. The grid in ζ-space most affects the results, especially for $c_2^{(0)}$ [compare the results by (S1,M1), (S1,M3), and (S1,M7), where M3 (or M1) is the grid about twice (or 3/2) as many points as M7]. The accuracy down to the fourth or fifth decimal place is expected from the table. The

comparisons among (S1,M1), (S3,M1), and (S1,M6) in the table show that the error due to the truncation of the ζ and η spaces is almost negligible.

The collision invariants are used to assess the accuracy of the collision integral computation, which is reduced to check the identities $C[(1,\mu\zeta,\zeta^2)E] = (1,\mu\zeta,\zeta^2)\nu E$ for $C = E\mathcal{C}E^{-1}$ and $C[E] = \nu E$ for $C = E\mathcal{C}^S E^{-1}$. With the standard grid M1, these identities are confirmed to hold within the error of 9.1×10^{-8}, 1.7×10^{-8}, 6.6×10^{-8}, and 8.9×10^{-9} respectively, while the maximum values of $(1,\mu\zeta,\zeta^2)\nu E$ are 0.13, 0.064, and 0.062 respectively.

The mass, momentum, and energy balances offer another measure of accuracy. They are the following identities that are obtained from (3.1a) and (3.2a) by the integration in molecular velocity space after multiplying the collision invariants:

$$\langle\mu\zeta\phi_2\rangle = \int_\eta^\infty Y_2^{(1)}(z)dz,\ \langle\mu^2\zeta^2\phi_2\rangle_+ = -\langle\mu^2\zeta^2\phi_2\rangle_-,$$

$$\langle\mu\zeta(\zeta^2-\frac{5}{2})\phi_2\rangle = \int_\eta^\infty H_2^{(1)}(z)dz, \tag{B.4a}$$

$$\langle\mu\zeta\phi_3\rangle = -\frac{1}{2}\int_\eta^\infty Y_1^{(1)}(z)dz,\ \langle\mu^2\zeta^2\phi_3\rangle_+ = -\langle\mu^2\zeta^2\phi_3\rangle_-,$$

$$\langle\mu\zeta(\zeta^2-\frac{5}{2})\phi_3\rangle = -\frac{1}{2}\int_\eta^\infty H_1^{(1)}(z)dz, \tag{B.4b}$$

$$\langle(\mu\zeta,\mu^2\zeta^2,\mu\zeta^3)\phi_5\rangle_+ = -\langle(\mu\zeta,\mu^2\zeta^2,\mu\zeta^3)\phi_5\rangle_-, \tag{B.4c}$$

$$\langle\mu(1-\mu^2)\zeta^3\psi_4\rangle_+ = -\langle\mu(1-\mu^2)\zeta^3\psi_4\rangle_-. \tag{B.4d}$$

Here $\langle\cdot\rangle_\pm$ is the half-range integral with respect to the molecular velocity defined by $\langle f(\boldsymbol{\zeta})\rangle_\pm = \langle f(\boldsymbol{\zeta})\chi[0,1](\pm\mu)\rangle$. $H_1^{(1)}$ and $H_2^{(1)}$ above have already appeared in (A.2) and are defined as $H_\beta^{(1)}(\eta) = (1/2)\langle\zeta^2(\zeta^2-5/2)(1-\mu^2)\psi_\beta\rangle$ ($\beta = 1,2$). With the standard grid (S1,M1), the identities in (B.4a) hold within the error of 3.2×10^{-8}, 8.1×10^{-7}, and 6.8×10^{-7}, while the maxima of their left-hand side are 0.48, 0.11, and 1.3. In the case of (B.4b), the error is within 4.3×10^{-7}, 7.8×10^{-8}, and 1.3×10^{-6}, while the maxima of the l.h.s. are 0.11, 0.055, and 0.076. In the case of (B.4c), the error is within 6.4×10^{-7}, 6.3×10^{-7}, and 4.7×10^{-6}, while the maxima of the l.h.s. are 0.085, 0.071, and 0.29. In the case of (B.4d), the error is within 3.6×10^{-6}, while the maximum of the l.h.s. is 0.14.

References

1. C. Bardos, R. E. Caflisch and B. Nicolaenko, The Milne and Kramers problems for the Boltzmann equation of a hard sphere gas, *Comm. Pure Appl. Math.*, **39** (1986), 323-352.

2. P. L. Bhatnagar, E. P. Gross and M. Krook, A model for collision processes in gases. I. small amplitude processes in charged and neutral one-component systems, *Phys. Rev.*, **94** (1954), 511-525.

3. S. Chapman and T. G. Cowling, *The Mathematical Theory of Non-uniform Gases*, Cambridge University Press, 3rd ed., Cambridge, 1991.

4. F. Golse, From the Boltzmann equation to the Euler equations in the presence of boundaries, *Comput. Math. Appl.*, **65** (2013), 815-830.

5. F. Golse and C. D. Levermore, Stokes–Fourier and acoustic limits for the Boltzmann equation: convergence proofs, *Comm. Pure Appl. Math.*, **55** (2002), 336-393.

6. F. Golse and L. Saint-Raymond, The Navier–Stokes limit of the Boltzmann equation for bounded collision kernels, *Invent. Math.*, **155** (2004), 81-161.

7. H. Grad, Asymptotic theory of the Boltzmann equation, *Phys. Fluids*, **6** (1963), 147-181.

8. D. Hilbert, Begründung der kinetischen Gastheorie, *Math. Ann.*, **72** (1912), 562-577.

9. M. Inaba, T. Yano and M. Watanabe, Linear theory of sound waves with evaporation and condensation, *Fluid Dyn. Res.*, **44** (2012), 025506.

10. N. Jiang, C. D. Levermore and N. Masmoudi, Remarks on the acoustic limit for the Boltzmann equation, *Comm. P. D. E.*, **35** (2010), 1590-1609.

11. E. H. Kennard, *Kinetic Theory of Gases*, McGraw-Hill, New York, 1938.

12. N. Masmoudi and L. Saint-Raymond, From the Boltzmann equation to the Stokes–Fourier system in a bounded domain, *Comm. Pure Appl. Math.*, **56** (2003), 1263-1293.

13. J. Nassios and J. E. Sader, Asymptotic analysis of the Boltzmann–BGK equation for oscillatory flows, *J. Fluid Mech.*, **708** (2012), 197-249.

14. T. Ohwada and Y. Sone, Analysis of thermal stress slip flow and negative thermophoresis using the Boltzmann equation for hard-sphere molecules, *Eur. J. Mech. B/Fluids*, **11** (1992), 389-414.

15. T. Ohwada, Y. Sone and K. Aoki, Numerical analysis of the shear and thermal creep flows of a rarefied gas over a plane wall on the basis of the linearized Boltzmann equation for hard-sphere molecules, *Phys. Fluids A*, **1** (1989), 1588-1599.

16. Y. Sone, Kinetic theory analysis of linearized Rayleigh problem, *J. Phys. Soc. Japan*, **19** (1964), 1463-1473.

17. Y. Sone, Asymptotic theory of flow of rarefied gas over a smooth boundary I, in *Rarefied Gas Dynamics*, edited by L. Trilling and H. Y. Wachman (Academic Press, New York, 1969), Vol. I, 243-253.

18. Y. Sone, Asymptotic theory of flow of rarefied gas over a smooth boundary II, in *Rarefied Gas Dynamics*, edited by D. Dini (Editrice Tecnico Scientifica, Pisa, 1971), Vol. II, 737-749.

19. Y. Sone, *Molecular Gas Dynamics*, Birkhäuser, Boston, 2007.

20. Y. Sone, T. Ohwada and K. Aoki, Temperature jump and Knudsen layer in a rarefied gas over a plane wall: numerical analysis of the linearized Boltzmann equation for hard-sphere molecules, *Phys. Fluids A*, **1** (1989), 363-370.

21. S. Takata, Symmetry of the linearized Boltzmann equation and its application, *J. Stat. Phys.*, **136** (2009), 751-784.

22. S. Takata, K. Aoki, M. Hattori and N. G. Hadjiconstantinou, Parabolic temperature profile and second-order temperature jump of a slightly rarefied gas in an unsteady two-surface problem, *Phys. Fluids*, **24** (2012), 032002.

23. S. Takata and H. Funagane, Poiseuille and thermal transpiration flows of a highly rarefied gas: over-concentration in the velocity distribution function, *J. Fluid Mech.*, **669** (2011), 242-259.

24. S. Takata and H. Funagane, Singular behaviour of a rarefied gas on a planar boundary, *J. Fluid Mech.*, **717** (2013), 30-47.

25. S. Takata and M. Hattori, Asymptotic theory for the time-dependent behavior of a slightly rarefied gas over a smooth solid boundary, *J. Stat. Phys.*, **147** (2012), 1182-1215.

26. P. Welander, On the temperature jump in a rarefied gas, *Ark. Fys.*, **7** (1954), 507-553.

27. S. Yasuda, S. Takata and K. Aoki, Numerical analysis of the shear flow of a binary mixture of hard-sphere gases over a plane wall, *Phys. Fluids*, **16** (2004), 1989-2003.

28. S.-H. Yu, Hydrodynamic limits with shock waves of the Boltzmann equation, *Comm. Pure Appl. Math.* **58** (2005), 409-443.